Nanoscale

PAPER

View Article Online
View Journal | View Issue

Cite this: *Nanoscale*, 2019, **11**, 3021

A piezo-phototronic enhanced serrate-structured ZnO-based heterojunction photodetector for optical communication†

Da Xiong,[a] Weili Deng,*[a] Guo Tian,[a] Yuyu Gao,[a] Xiang Chu,[a] Cheng Yan,[a] Long Jin,[a] Yuhan Su,[a] Wei Yan[b] and Weiqing Yang *[a,c]

ZnO-based heterojunction photodetectors have been widely used in various fields such as optical imaging and health monitoring. As for the traditional planar heterojunction interface, their limited optical absorption will place restrictions on the full photoelectric potential of ZnO nanorods, which severely restrains the commercial applications of ZnO-based photodetectors. Herein, using an intrinsically octahedral structure of p-type Cu_2O and one-dimensional ZnO arrays, the newly designed serrate-structured heterojunction was constructed, whose unique serrate-structured interface of ZnO/Cu_2O is highly conducive to the aggrandizing of optical absorption. The as-fabricated photodetector could achieve a high on/off ratio up to 1000 and an optimum photocurrent of 24.90 μA under 1.41 mW mm^{-2} (405 nm) illumination without bias voltage, which was 2.5 times higher than that of the planar-structured photodetector, and the response time was as quick as 1.6 ms. When the additional external strain was 0.39%, the performance was dramatically enhanced more than 5 times due to the synergism of the piezo-phototronic effect and the serrate-structured design. Based on this, we successfully developed designed photodetector arrays with an excellent optical communication performance of transmitting information. Prospectively, this kind of unique serrate-structured heterojunction design will open up a possible opportunity for high performance photodetectors based on structural engineering.

Received 21st November 2018,
Accepted 14th January 2019

DOI: 10.1039/c8nr09418g

rsc.li/nanoscale

Introduction

As one of the most important parts of optoelectronic devices, photodetectors have been widely used in various areas such as fire detection, optical imaging, optical communication, and so on.[1–7] Among them, the photovoltaic based photodetector is the most promising device to realize high sensitivity and rapid detection without bias voltage due to the existence of the built-in electric field.[8,9] Typically, zinc oxide (ZnO)-based heterojunction photodetectors[10–13] have attracted a great deal of attention owing to their unique semiconductor characteristics (a wide direct bandgap of 3.37 eV and a high exciton binding energy of 60 meV),[14,15] piezoelectric effects,[16,17] and photonic and photoelectric effects.[18–20] Besides, the unique one-dimensional structure of ZnO nanorods can shorten the transmission time of carriers for a high responsivity in photodetectors.[21–23] So far, the heterojunction interface structure of ZnO-based photodetectors has been mainly planar.[24–27] Although these kinds of photodetectors can obtain the higher photoelectric performance, their limited optical absorption places restrictions on the full photoelectric potential of ZnO nanorods, which severely restrains the commercial applications of ZnO-based photodetectors.

Here, we employed serrate-structured p-type cuprous oxide (Cu_2O) to construct the unique serrate-structured interface of the heterojunction for the newly designed serrate-structured ZnO/Cu_2O photodetectors (SZCPs), whose serrated structure is so useful to significantly aggrandize the optical absorption. By making clever use of the intrinsically octahedral structure of Cu_2O, the serrate structure of the device can be effectively regulated by process conditions, which can helpfully simplify the preparation process. Meanwhile, Cu_2O is a typical p-type semiconductor with an attractive direct band-gap of 2.0 eV,[28,29] which contributes to the construction of the pn junction with

[a]*Key Laboratory of Advanced Technologies of Materials (Ministry of Education), School of Materials Science and Engineering, Southwest Jiaotong University, Chengdu 610031, China. E-mail: weili1812@swjtu.edu.cn, wqyang@swjtu.edu.cn*
[b]*State Key Laboratory of Optical Technologies for Microfabrication, Institute of Optics and Electronics, Chinese Academy of Sciences, Chengdu 610209, China*
[c]*State Key Laboratory of Traction Power, Southwest Jiaotong University, Chengdu 610031, China*

†Electronic supplementary information (ESI) available: The cross-sectional SEM image of Cu_2O; the SEM images of ZnO nanorods synthesized on the surface of Cu_2O; the stability of the photodetector and its schematic diagram; the photoresponse behaviors of the photodetector with different strains; the comparison of the performance of ZnO-based photodetectors; the application of optical switch under laser illumination; the application of optical switch under light illumination. See DOI: 10.1039/c8nr09418g

n-type ZnO nanorods to realize self-powered photodetection. Above all, this serrate-structured ZnO-based photodetector demonstrates a high on/off ratio up to 1000 and an optimum photocurrent of 24.90 μA under 1.41 mW mm^{-2} (405 nm) illumination; the response time was as quick as 1.6 ms, which reveals that the designed serrate-structured interface can undoubtedly enhance the performance of the ZnO-based heterojunction photodetectors. In addition, due to the piezoelectric properties of ZnO, the performance of the serrate-structured heterojunction photodetector was further optimized by more than 2 times with the piezo-phototronic effect.[30–33] In other words, the performance can be overall enhanced by 5 times compared with the planar-structured photodetector. More interestingly, the applications of the optical switch and the optical communication were further successfully demonstrated based on the as-fabricated SZCPs. In prospect, this work provides a practicable pathway to improve the performance of the photodetectors by structural engineering.

Experimental section

The preparation of Cu_2O

The method of electrochemical deposition was selected to fabricate a Cu_2O film, which was carried out using a three-electrode cell; Hg/HgO and platinum were used as the reference electrode and the counter electrode, while the poly(ethylene naphthalate)-indium tin oxide (PEN-ITO) substrate was used as the working electrode. The electrochemical deposition potential was controlled at −0.45 V *vs.* Hg/HgO, using the CHI660E electrochemical workstation. The preparation process was maintained at 313 K using a water bath system. The Cu_2O layer was deposited on the substrate using the electrolyte solution consisting of 0.02 M copper sulfate and 0.4 M lactic acid; what's more, the pH of the solution was adjusted to 12–13 using 1 M sodium hydroxide.[18] The deposition time was controlled at 0.5, 1.0 and 1.5 h, respectively. Then the deposited Cu_2O film was washed with deionized water three times and dried at 333 K for half an hour.

The preparation of the ZnO nanorod

It has been reported that a ZnO seed layer can help to reduce the mismatch between the nanorods and the substrate; on the other hand, by means of the seed layer, the quality of the growing ZnO nanorods will be better.[34] So we started making the nanorods by depositing a ZnO seed layer using radio frequency magnetron sputtering technology. The growth solution of the nanorods contains hexamethylenetetramine (HMTA) and zinc nitrate ($Zn(NO_3)_2{\cdot}6H_2O$); the concentration of it was 0.1 M and the preparation process was carried out by a chemical bath deposition method at 358 K for 6 h. Then the film was washed with deionized water and dried at 358 K.

The preparation of the photodetector

Before making the electrode of the photodetector, we spun a thin organic polymer polymethyl methacrylate (PMMA) as a protective layer, which can protect the ZnO nanorods from breaking under large strain. Then the Ag electrode was sputter coated on the heterojunction as the top electrode to form the sandwich structure.

Characterization

The morphologies of both the Cu_2O and the ZnO nanorod layers were characterized by using a field emission scanning electron microscope (FESEM JSM7800F). The crystal structure of the film was examined by X-ray diffraction (XRD X'pert Powder) at 40 kV and 40 mA using Cu Kα radiation. The volt–ampere characteristics of the photodetectors were determined by using a Keithley 4200 semiconductor testing system, and the photoelectric performance characterization was carried out by using a Stanford SR570 Preamplifier. The light source was provided by lasers which were controlled by using a function signal generator.

Results and discussion

Fig. 1 schematically demonstrates the structure design and the potential optical communication application of SZCPs. The construction of serrate-structured ZnO-based heterojunction photodetectors is schematically presented in Fig. 1a. The n-type ZnO nanorods were synthesized along the surface of serrated p-type Cu_2O to form the serrate-structured interface of the pn junction. Then, a thin organic polymer film (PMMA) was spin-coated onto the heterojunction as a protective layer.

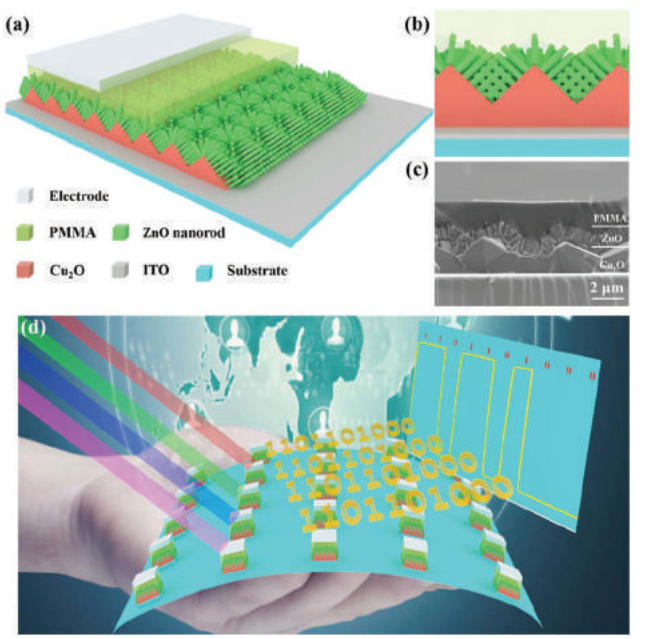

Fig. 1 (a) Schematic illustration showing the serrate-structured ZnO/Cu_2O heterojunction based photodetector. (b) Schematic illustration of the structure between ZnO nanorods and Cu_2O. (c) Cross-sectional SEM image of the corresponding heterojunction. (d) The schematic diagram of optical communication based on the designed photodetector arrays.

Finally, the evaporated silver electrode and the original (ITO) electrode on flexible and transparent PEN substrates firmly sandwiched on both sides of the serrate-structured ZnO-based heterojunction (the detailed preparation process can be found in the Experimental section). Furthermore, the cross-sectional schematic and scanning electron microscopy (SEM) images of the heterojunction are contrastively presented in Fig. 1b and c, respectively. The serrate-structured heterojunction interface was successfully constructed when the ZnO nanorods were vertically grown on the surface of serrate-structured Cu_2O. Based on this, the photodetector arrays used for optical communication were further developed and displayed in Fig. 1d. It can be seen when light is irradiated on the device, photocurrent will be generated by the SZCP, that is, the optical signals are converted into electrical signals. If the optical signal changes in a certain way to encode information, then the corresponding information can be decoded by the electric output of the photodetectors. Furthermore, combined with the excellent performance of photodetector arrays, multi-channel transmission of signals can be realized, which could play an important role of communication in our future life.

To confirm the role of the designed serrate-structured interface on improving the performance of ZnO-based heterojunction photodetectors, the heterojunction interfaces with different serrated degrees were exploited and characterized. As shown in Fig. 2a–c, when the electrochemical deposition time was 0.5 h, Cu_2O showed almost no serrated appearance (Fig. 2a), but the surface of Cu_2O showed the best serrated structure (Fig. 2b) after increasing the deposition time to 1.0 h; the thickness of Cu_2O was about 2.0 μm (Fig. S1†); however when the deposition time was continuously prolonged to 1.5 h, the surface of the fabricated Cu_2O gradually became flat owing to the vacancies which were filled with a small sized grain of Cu_2O. The deposited ZnO seeds are uniformly distributed on the surface (Fig. 2d), which is ascribed to the growth of ZnO nanorods along only one lattice plane. Hence, the as-fabricated ZnO nanorod array grows vertically along the serrated surface of Cu_2O (Fig. 2e), which is good for achieving the serrate-structured interface. Compared with the top view of the fabricated pn junction with different deposition times (Fig. S2†), it can be found that the surface morphology of the as-synthesized ZnO nanorods still depends on the morphology of Cu_2O. Moreover, the serrated interface of the heterojunction was further evidently demonstrated by the cross-sectional SEM image (Fig. 2f).

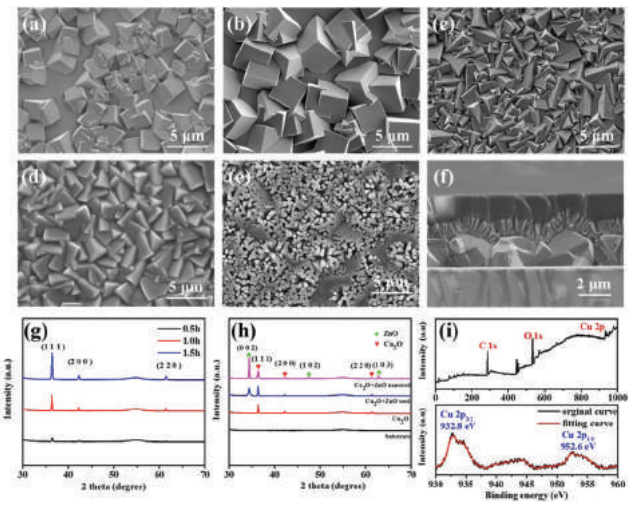

Fig. 2 (a)–(c) SEM image of Cu_2O with different deposition times of 0.5, 1.0 and 1.5 h. SEM images of (d) Cu_2O–ZnO seeds and (e) Cu_2O–ZnO nanorods. (f) The cross-sectional SEM image of the ZnO/Cu_2O heterojunction. (g) XRD pattern of Cu_2O with different deposition times. (h) XRD pattern of the serrate-structured ZnO/Cu_2O heterojunction. (i) XPS survey spectrum of the fabricated serrate-structured ZnO/Cu_2O heterojunction and the core level spectrum of Cu 2p in Cu_2O.

To further characterize the crystal structure of the heterojunction, the fabricated pn junctions were characterized by the X-ray diffraction technique (XRD). Fig. 2g shows the XRD pattern of Cu_2O with different deposition times, which obviously reveals the preferred Cu_2O crystal orientation of (111) at $2\theta = 36.4°$. In addition, the observed diffraction peaks at 42.3° and 61.4° should be assigned to the (200) and (220) planes of Cu_2O (JCPDS 99-0041). By means of the XRD pattern of the heterojunction (Fig. 2h), the (002), (102) and (103) planes at the diffraction peaks of 34.4°, 47.5° and 62.8° evidently identified the hexagonal ZnO crystalline phase with a wurtzite structure (JCPDS 99-0111). Besides, X-ray photoelectron spectroscopy (XPS) was further used to confirm the chemical state of the Cu element in the fabricated film (Fig. 2i). In the Cu 2p core level spectrum, the peaks of Cu $2p_{3/2}$ (932.8 eV) and Cu $2p_{1/2}$ (952.6 eV) obviously demonstrate that the fabricated layer was Cu_2O rather than CuO and Cu.[28,35]

In order to further characterize the performance of the as-fabricated photodetectors, the test platform was constructed through a displacement machine, function signal generator, laser and current preamplifier (Fig. 3a). As can be seen from Fig. 3b and c, all fabricated heterojunctions exhibited good rectifier characteristics, indicating the well-defined pn junction at the interface between ZnO and Cu_2O; the inset image of Fig. 3b shows the semiconductor properties of ZnO nanorods. The serrate-structured heterojunction shows the optimum photocurrent up to 24.90 μA under light of 405 nm at 1.41 mW mm^{-2} illumination without bias voltage, which is about 2.5 times higher than that of the planar-structured heterojunction. It indeed demonstrates that this newly designed serrated structure could greatly enhance the performance of photodetectors. Moreover, the on/off ratio of current exceeded 1000 without any extra supply source, obviously rendering the excellent photosensitive characterization of the designed photodetector compared with the results of other literature studies[20,36] (the corresponding comparison of the photoresponse is shown in Tables S1 and S2†). Meanwhile, even if the duty cycle of the laser on and off changed from 20%–80%, the amplitude of the photocurrent still remains unchanged (Fig. 3d), obviously presenting the high photoelectric detection sensitivity. Additionally, to further investigate the durability of the as-fabricated photodetector, a repetitive irradiation test of more than

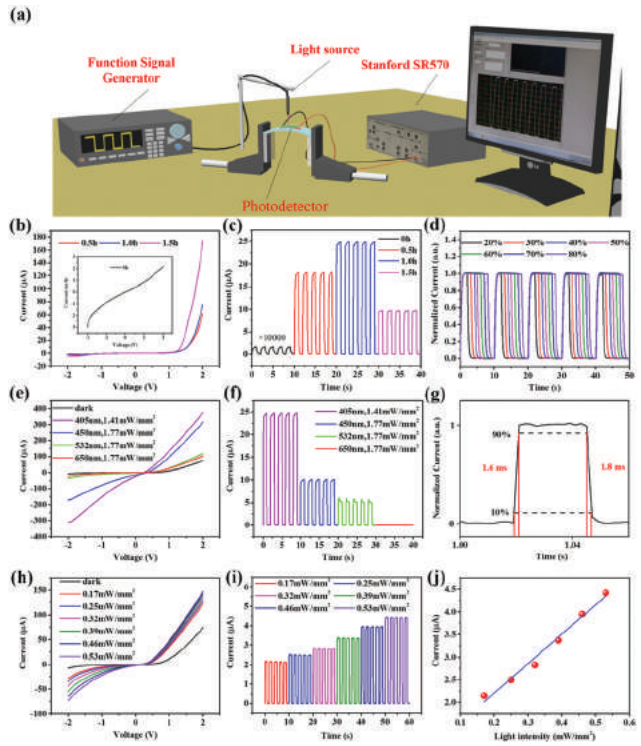

Fig. 3 (a) Experimental platform for measuring the optical responses and modulation with strains. (b) *I–V* characteristics of the photodetectors with different morphologies. The inset shows the *I–V* characteristics of ZnO nanorods. (c) Photoresponse behaviors of the photodetectors with different morphologies without bias voltage under 405 nm (1.41 mW mm^{-2}) illumination. (d) Photoresponse behaviors of the photodetector under different duty cycles of laser on and off. (e) *I–V* characteristics and (f) photoresponse behaviors of the photodetector at different light wavelengths of 405 nm (1.41 mW mm^{-2}), 450, 532 and 650 nm (1.77 mW mm^{-2}). (g) The response time of the designed photodetector. (h) *I–V* characteristics and (i) photoresponse behaviors of the photodetector under 405 nm illumination with different light intensities. (j) The photoresponse behaviours of the photodetector as a function of the light intensity.

2500 cycles was carried out under light of 405 nm at 1.41 mW mm^{-2} illumination without bias voltage. As shown in Fig. S3a,† the result exhibits the good stability of SZCPs, which turns out a certain lifetime of practical application, and their parameters remain almost unchanged after 4000 s uninterrupted illumination (Fig. S3b†).

To further characterize the performance of the designed photodetector under different light illumination conditions, we selected the best serrate-structured heterojunction photodetector to carry out the performance test the performance test under the wavelengths of 405, 450, 532 and 650 nm illumination. As displayed in Fig. 3e and f, its photocurrent decreases with the increase of the visible light wavelength. Meanwhile, the serrate-structured photodetector could realize a quick response, compared with the photodetector based on the photoconductive effect,[37–39] whose rise/fall time, defined as the time required for the photocurrent to increase/decrease from 10% to 90% of its peak value, was 1.6 and 1.8 ms, respectively, as shown in Fig. 3g. According to the *I–V* curves under different light intensities (Fig. 3h), the photodetector shows a stronger photoresponse with positive bias. Besides, from Fig. 3i and j, the photoresponse behaviour of the photodetector reveals that the photocurrent is proportional to the light intensity under the same light wavelength of 405 nm illumination when the light intensity ranges from 0.17 to 0.53 mW mm^{-2}.

The newly designed SZCPs have merits in extraordinary performance and simplified preparation process. Firstly, the serrate-structured design greatly provides multiple reasons for the improved performance of the photodetectors. The serrate-structured design causes scattering of light over a large angular range and increases the specific surface area of the heterojunction, resulting in sufficient light absorption.[40] Secondly, the serrate-structured design could contribute to improving the stability of devices, because it can help to avoid the materials peeling and breaking, exactly as shown in Fig. S4.† In addition, the construction of the serrated interface was based on the intrinsically octahedral structure of Cu_2O, which simplified the manufacturing process and reduced the production costs. Besides, all the experimental methods can be used in mass and rapid production. The low-cost and ordinary fabrication process of SZCPs can effectively promote their commercial applications.

To further explore the photoelectric performance of the designed SZCPs, the piezo-phototronic effect was then introduced to modulate the band structure of the fabricated pn junction. Experimentally, Fig. 4a and b show that the dark current decreases with the increase of the compressive strain at the same bias voltage. The relevant conclusion can be explained by following theoretical analysis of change in the energy band when a compressive strain was applied on a pn junction, as shown in Fig. 4c and d. In detail, due to the piezoelectric effect of ZnO, the positive piezo-charges are produced at the ZnO/Cu_2O heterojunction interface under compressive strain, leading to the holes in the p-type Cu_2O moving toward but the electron in the n-type ZnO away from the pn junction interface. The depletion region shifts from the initial gray region to the blue region[41] and the energy band at both sides will bend downward (blue dashed line), resulting in the increase of the barrier height of the heterojunction,[31] thus the dark current decreases at the same bias voltage when compressive strain is being applied. Furthermore, the influence of the compressive strain on the photoelectric performance of the designed SZCPs was systematically investigated at different light wavelengths. When the photodetector worked under light of 405 nm at 1.41 mW mm^{-2} illumination without bias voltage, the photocurrent as a function of compressive strain from 0% to 0.45% is displayed in Fig. 4e, clearly demonstrating the enhanced photoelectric performance of the piezo-phototronic effect. When compressive strain was 0.39%, the photodetector achieved the maximum output, which is about 2.16 times higher than that without any compressive strain. In other words, the performance of the ZnO-based photodetectors could be enhanced by about 5 times under the syner-

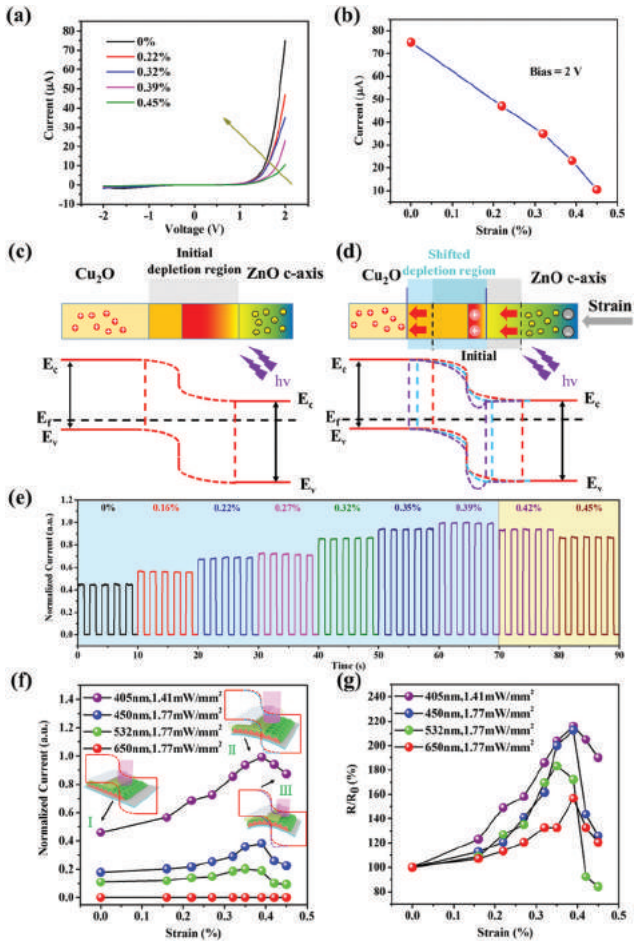

Fig. 4 (a) *I–V* characteristics of the photodetector with different compressive strains under dark conditions. (b) Current changes with the external strains at 2 V bias. The energy band diagram of the Cu_2O/ZnO heterojunction (c) without strain, and (d) with compressive strain. The red, blue and purple dashed lines show the energy band at different stages: illumination without strains, illumination with small strain, and illumination with large strain, respectively. (e) The photoresponse behaviours of the photodetector with different strains under 1.41 mW mm^{-2} (405 nm) illumination. (f) Photocurrent and (g) R/R_0 of the photodetector with different strains under 405 nm (1.41 mW mm^{-2}) and 450, 532, and 650 nm (1.77 mW mm^{-2}) illumination.

gistic effect of the serrated structure design and the piezo-phototronic effect. However, the photocurrent would decrease with the further increase of the compressive strain; the detailed explanation of the deterioration of the performance will be discussed later. The similar results can also be found when the fabricated serrate-structured photodetector was exposed to the light of 450, 532 or 650 nm at 1.77 mW mm^{-2} (Fig. S5†). Under different light sources, the photocurrent and the relative changes of responsivity R (with compressive strain) with respect to R_0 (without compressive strain) varying with different compressive strains from 0% to 0.45% are depicted in Fig. 4f and g (the responsivity R defined as $R = I_{ph}/P_{in}$, I_{ph} is the photocurrent, and P_{in} is the light intensity), respectively. It is observed that the R/R_0 values varied with the applied strain in a similar strain-dependence profile to that of the photocurrent under each light wavelength illumination: the performance first increases to a maximum value when applied with appropriate compressive strain, and then decreases to a certain extent when it continues to increase.

The strain-independence tendency of the photocurrent can be attributed to the following reasons. When there is no strain applied (I in Fig. 4f), the increase of the photocurrent depends on the separation and collection of the photo-induced electron–hole pairs by the built-in electric field at the pn junction. When a mechanical strain is applied to the device, the positive piezoelectric charge generates at the interface of the SZCP, which induces a sharper and extended built-in electric field just like an externally applied positive bias voltage. The enhanced built-in electric field would more effectively promote the separation of the photo-induced electron hole pairs for the improved photovoltaic effect and higher photocurrent.[18,42] Therefore, the increase in the photocurrent was observed until the maximum value (II in Fig. 4f) with the applied compressive strain. However, when the applied compressive strain was further increased, the downward bend of the energy band is so significant that a new energy barrier/trap appears at the interface of the SZCP (purple dashed line in Fig. 4d). The nascent energy band suppresses the separation of photo-induced electron–hole pairs,[43,44] which is in contrast with the amplification of the photocurrent by the enhanced built-in electric field. Therefore, the overall photodetector performance begins to decrease under large compressive strain (III in Fig. 4f). However, with the increase of the light wavelength, the increase in the rate of the photocurrent gradually decreases (Fig. 4g), which can be attributed to the decrease of the screening effect under weak illumination and the stronger effect of polarization charges at the interfaces when being applied to the compressive strain. The positive polarization can attract and trap more photo-induced electrons, which leads to the decrease of the photocurrent, and thus the modulation ability of the piezo-phototronic effect is weakened.[36] Such a phenomenon clearly shows that the strain can significantly modulate the band structure at the interface by affecting the charge carrier transport, separation and recombination process.

The excellent photoelectric performance of SZCPs makes them good candidates for optical transducers like optical switches and optical communication. Fig. 5a presents the schematic circuit diagram of the photodetector as an optical switch. When the photodetector received light, the resistance of the photodetector would decrease due to the production of photocurrent. Hence, the voltage distributed in the series resistance would increase, resulting in the LED blinking or shinning. This means the state of the LED can be controlled by light, and the function of the optical switch is realized. From the practical experiment, as shown in Fig. 5b, when the photodetector was exposed to purple light, the LED began to blink, and after taking away the light source, the LED would stop blinking. What's more, when the surroundings changed from natural light to dark, we could adjust the resistance value of R_1 to control the threshold of the device for different applications

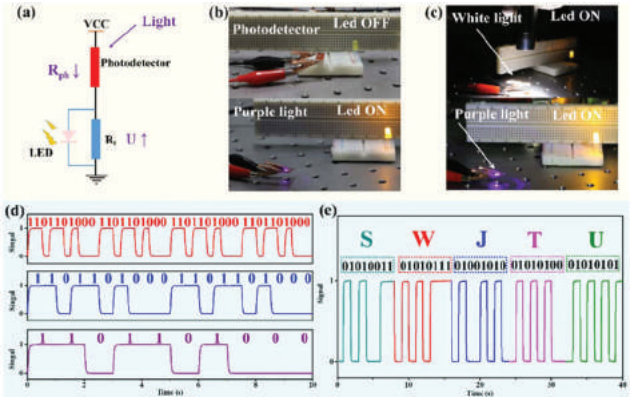

Fig. 5 The applications of the SZCPs. (a) The circuit of the photodetector used as an optical switch. The photos of the optical switch working under different situations of (b) natural light and (c) dark. (d) The response of the photodetector used in optical communication with different frequencies. (e) The decode procedure of the photodetector used in optical communication according to the ASCII code.

(Fig. 5c). Similarly, whether these SZCPs can be triggered by the light or not can be seen from Videos 1 and 2 in the ESI†.

More interestingly, due to the characteristics of the photodetector, when it is exposed to light, there is an electrical output, otherwise there is nothing. Then, when setting a specific threshold for the electrical output to represent "1" or "0", its coding can be realized by controlling the state of illumination. On the other hand, the corresponding decoding would also be realized through distinguishing the output of the electric signal for the high electric output or the low electric output according to the threshold. Besides, due to the fast response of the photodetector, the encoding process would not be influenced even if the frequency of the code is changed, as demonstrated in Fig. 5d. Moreover, if the coding is in accordance with the rules of the American Standard Code for Information Interchange (ASCII), it results in "01010011", "01010111", "01001010", "01010100" and "01010101" which represent "S", "W", "J", "T" and "U", respectively, which successfully demonstrated the application of the optical communication based on SZCPs (Fig. 5e). After converting the optical message into the electric output, the influence of information transmission caused by the limited propagation distance of light can be effectively shielded, which served the purpose of reducing the interference signal during transmission, resulting in promoting the signal to noise ratio. Above all, it is an attractive prospect that the photodetectors can be used in optical communication.

Conclusions

In summary, we newly designed a serrate-structured ZnO-based heterojunction photodetector. Due to this unique serrate-structured ZnO/Cu_2O interface effect, the as-fabricated photodetector could reach the optimum photocurrent of 24.90 μA under 1.41 mW mm^{-2} (405 nm) illumination without bias voltage, which was 2.5 times higher than that of the planar-structured photodetector. With the additional external stress of 0.39%, the dramatically enhanced photocurrent of this photodetector was about 5 times that of the ZnO-based planar-structured photodetector, which is mainly ascribed to the synergism of the piezo-phototronic effect and the serrated structured design. In addition, the serrate-structured photodetectors showed a rapid response time of 1.6 ms and the on/off ratio up to 1000. Based on this, we successfully developed designed photodetector arrays with an excellent optical communication performance to transmit information encoded under the rule of ASCII. Generally, this design of the serrate-structured interface of the heterojunction provided a feasible approach to effectively enhance the photoelectric performance of the photodetectors and opened a new way to exploit the next generation of photoelectric function heterojunctions.

Conflicts of interest

There are no conflicts to declare.

Acknowledgements

This work was financially supported by the National Natural Science Foundation of China (No. 61801403), the Scientific and Technological Projects for International Cooperation of Sichuan Province (No. 2017HH0069), the Independent Research Project of State Key Laboratory of Traction Power (No. 2017TPL_Z04), and the Fundamental Research Funds for the Central Universities of China (No. 2682017CY06, 2682017ZDPY01 and 2682017ZDPY01). Thanks for the help from the Analysis and Testing Center of Southwest Jiaotong University.

Notes and references

1 H. Tetsuka, *Sci. Rep.*, 2017, **7**, 5544.
2 X. Han, W. Du, R. Yu, C. Pan and Z. L. Wang, *Adv. Mater.*, 2015, **27**, 7963–7969.
3 L. Gu, M. M. Tavakoli, D. Zhang, Q. Zhang, A. Waleed, Y. Xiao, K. H. Tsui, Y. Lin, L. Liao, J. Wang and Z. Fan, *Adv. Mater.*, 2016, **28**, 9713.
4 C. Xie and F. Yan, *Small*, 2017, **13**, 1701822.
5 S. Chen, Z. Lou, D. Chen and G. Shen, *Adv. Mater.*, 2018, **30**, 1705400.
6 M. Rein, V. D. Favrod, C. Hou, T. Khudiyev, A. Stolyarov, J. Cox, C. C. Chung, C. Chhav, M. Ellis, J. Joannopoulos and Y. Fink, *Nature*, 2018, **560**, 214–218.
7 S. C. Dhanabalan, J. S. Ponraj, H. Zhang and Q. Bao, *Nanoscale*, 2016, **8**, 6410–6434.
8 M. Buscema, J. O. Island, D. J. Groenendijk, S. I. Blanter, G. A. Steele, H. S. van der Zant and A. Castellanos-Gomez, *Chem. Soc. Rev.*, 2015, **44**, 3691–3718.

9 F. Zhuge, Z. Zheng, P. Luo, L. Lv, Y. Huang, H. Li and T. Zhai, *Adv. Mater. Technol.*, 2017, **2**, 1700005.
10 Z. Zhang, Q. Liao, Y. Yu, X. Wang and Y. Zhang, *Nano Energy*, 2014, **9**, 237–244.
11 X. Zheng, Y. Sun, X. Yan, X. Chen, Z. Bai, P. Lin, Y. Shen, Y. Zhao and Y. Zhang, *RSC Adv.*, 2014, **4**, 18378.
12 J. Sun, X. Zhang, Y. Lang, J. Bian, R. Gao, P. Li, Y. Wang and C. Li, *Nano Energy*, 2017, **32**, 96–104.
13 T. Park, K. E. Lee, N. Kim, Y. Oh, J.-K. Yoo and M.-K. Um, *J. Mater. Chem. C*, 2017, **5**, 12256–12263.
14 S. M. Hatch, J. Briscoe and S. Dunn, *Adv. Mater.*, 2013, **25**, 867–871.
15 C. Liu, M. Peng, A. Yu, J. Liu, M. Song, Y. Zhang and J. Zhai, *Nano Energy*, 2016, **26**, 417–424.
16 W. Deng, L. Jin, B. Zhang, Y. Chen, L. Mao, H. Zhang and W. Yang, *Nanoscale*, 2016, **8**, 16302–16306.
17 Y. Zhang, C. Liu, J. Liu, J. Xiong, J. Liu, K. Zhang, Y. Liu, M. Peng, A. Yu, A. Zhang, Y. Zhang, Z. Wang, J. Zhai and Z. L. Wang, *ACS Appl. Mater. Interfaces*, 2016, **8**, 1381–1387.
18 P. Lin, X. Chen, X. Yan, Z. Zhang, H. Yuan, P. Li, Y. Zhao and Y. Zhang, *Nano Res.*, 2014, **7**, 860–868.
19 S. Lim, D.-S. Um, M. Ha, Q. Zhang, Y. Lee, Y. Lin, Z. Fan and H. Ko, *Nano Res.*, 2016, **10**, 22–36.
20 M. Chen, B. Zhao, G. Hu, X. Fang, H. Wang, L. Wang, J. Luo, X. Han, X. Wang, C. Pan and Z. L. Wang, *Adv. Funct. Mater.*, 2018, **28**, 1706379.
21 L. Peng, L. Hu and X. Fang, *Adv. Mater.*, 2013, **25**, 5321–5328.
22 Z. Zheng, L. Gan, J. Zhang, F. Zhuge and T. Zhai, *Adv. Sci.*, 2017, **4**, 1600316.
23 Z. Lou and G. Shen, *Adv. Sci.*, 2016, **3**, 1500287.
24 L. P. Zhu, Y. Zhang, P. Lin, Y. Wang, L. J. Yang, L. B. Chen, L. F. Wang, B. D. Chen and Z. L. Wang, *ACS Nano*, 2018, **12**, 1811–1820.
25 F. Zhang, S. M. Niu, W. X. Guo, G. Zhu, Y. Liu, X. L. Zhang and Z. L. Wang, *ACS Nano*, 2013, **7**, 4537–4544.
26 Q. Liao, M. Liang, Z. Zhang, G. Zhang and Y. Zhang, *Nano Res.*, 2015, **8**, 3772–3779.
27 F. X. Liang, Y. Gao, C. Xie, X.-W. Tong, Z. Li and L. Luo, *J. Mater. Chem. C*, 2018, **6**, 3815–3833.
28 X. Liu, H. Du, P. Wang, T.-T. Lim and X. W. Sun, *J. Mater. Chem. C*, 2014, **2**, 9536–9542.
29 Z. Kang, X. Yan, Y. Wang, Z. Bai, Y. Liu, Z. Zhang, P. Lin, X. Zhang, H. Yuan, X. Zhang and Y. Zhang, *Sci. Rep.*, 2015, **5**, 7882.
30 Z. L. Wang, R. Yang, J. Zhou, Y. Qin, C. Xu, Y. Hu and S. Xu, *Mater. Sci. Eng., R*, 2010, **70**, 320–329.
31 W. Peng, X. Wang, R. Yu, Y. Dai, H. Zou, A. C. Wang, Y. He and Z. L. Wang, *Adv. Mater.*, 2017, **29**, 1606698.
32 W. Wu and Z. L. Wang, *Nat. Rev. Mater.*, 2016, **1**, 16031.
33 Z. L. Wang, *Nano Today*, 2010, **5**, 540–552.
34 M. Guo, P. Diao and S. Cai, *J. Solid State Chem.*, 2005, **178**, 1864–1873.
35 Y. J. Chen, M. H. Li, J. C. Huang and P. Chen, *Sci. Rep.*, 2018, **8**, 7646.
36 H. Zou, X. Li, W. Peng, W. Wu, R. Yu, C. Wu, W. Ding, F. Hu, R. Liu, Y. Zi and Z. L. Wang, *Adv. Mater.*, 2017, **29**, 1701412.
37 F. Xue, L. Chen, J. Chen, J. Liu, L. Wang, M. Chen, Y. Pang, X. Yang, G. Gao, J. Zhai and Z. L. Wang, *Adv. Mater.*, 2016, **28**, 3391–3398.
38 K. Liu, M. Sakurai, M. Aono and D. Shen, *Adv. Funct. Mater.*, 2015, **25**, 3157–3163.
39 X. Zhou, Q. Zhang, L. Gan, H. Li and T. Zhai, *Adv. Funct. Mater.*, 2016, **26**, 4405–4413.
40 P. Xiao, J. Mao, K. Ding, W. Luo, W. Hu, X. Zhang, X. Zhang and J. Jie, *Adv. Mater.*, 2018, **30**, 1801729.
41 Y. Dai, X. Wang, W. Peng, H. Zou, R. Yu, Y. Ding, C. Wu and Z. L. Wang, *ACS Nano*, 2017, **11**, 7118–7125.
42 J. Shi, P. Zhao and X. Wang, *Adv. Mater.*, 2013, **25**, 916–921.
43 W. Wu, L. Wang, R. Yu, Y. Liu, S. H. Wei, J. Hone and Z. L. Wang, *Adv. Mater.*, 2016, **28**, 8463–8468.
44 W. Wu, L. Wang, Y. Li, F. Zhang, L. Lin, S. Niu, D. Chenet, X. Zhang, Y. Hao, T. F. Heinz, J. Hone and Z. L. Wang, *Nature*, 2014, **514**, 470–474.